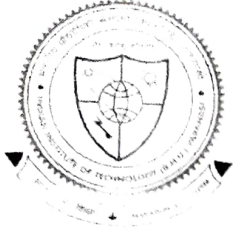
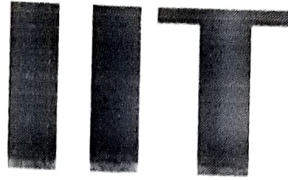


*Dedicated to my Beloved Parents and  
Family*



भारतीय  
प्रौद्योगिकी  
संस्थान



INDIAN  
INSTITUTE OF  
TECHNOLOGY  
BANARAS HINDU UNIVERSITY

### CERTIFICATE

It is certified that the work contained in the thesis titled *Tuning of Redox energies of transition metal ions in different lattices for grid-scale energy storage applications* by "RAKESH MONDAL" has been carried out under my supervision and that this work has not been submitted elsewhere for a degree.

It is further certified that the student has fulfilled all there quirements of the comprehensive examination, candidacy, and SOTA for the award of Ph.D. Degree.

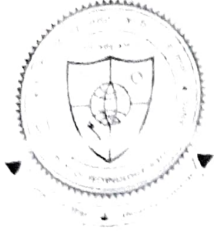
Dr. Preetam Singh  
Supervisor  
Assistant Professor,  
Department of Ceramic Engineering,  
Indian Institute of Technology (BHU),  
Varanasi - 221005, (U.P.),

भारतीय प्रौद्योगिकी संस्थान (का०हि०वि०वि०)  
Varanasi-221005/वाराणसी-221005

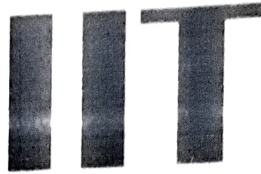
Dr. Anil Kumar  
Co-Supervisor  
Associate Professor  
Department of Ceramic Engineering,  
Indian Institute of Technology (BHU),  
Varanasi - 221005, (U.P.), India

भारतीय प्रौद्योगिकी संस्थान (का०हि०वि०वि०)  
Varanasi-221005/वाराणसी-221005

Prof. Vinay Kumar Singh  
Head of Department  
HEAD/विभागाध्यक्ष  
Department of Ceramic Engineering,  
Indian Institute of Technology (BHU)  
सिरीमिक अभियान्तिकी विभाग  
Indian Institute of Technology (B.H.U.), India  
भारतीय प्रौद्योगिकी संस्थान (का०हि०वि०वि०)  
Varanasi-221005/ वाराणसी-221005



भारतीय  
प्रौद्योगिकी  
संस्थान  
काशी हिन्दू विश्वविद्यालय



INDIAN  
INSTITUTE OF  
TECHNOLOGY  
BANARAS HINDU UNIVERSITY

### DECLARATION BY THE CANDIDATE

I, **Rakesh Mondal**, certify that the work embodied in this thesis is my own bonafide work carried out by me under the supervision of **Dr. Preetam Singh** from **July 2016 to July 2022**, at the **Department of Ceramic Engineering**, Indian Institute of Technology (BHU), Varanasi. The matter embodied in this thesis has not been submitted for the award of any other degree/diploma.

I declare that I have faithfully acknowledged and given credits to the research workers wherever their works have been cited in my work in this thesis. I further declare that I have not will fully copied any other's work, paragraphs, text, data, results, etc., reported in journals, books, magazines, reports dissertations, thesis, etc., or available on websites and have not included them in this thesis and have not cited as my own work.

**Rakesh Mondal**  
Signature of the student

(Rakesh Mondal)

Date:

Place: IIT (BHU), Varanasi

### CERTIFICATE BY THE SUPERVISOR

It is certified that the above statement made by the student is correct to the best of my/our knowledge.

**Dr. Preetam Singh**  
Supervisor

Assistant Professor,

Department of Ceramic Engineering,

Indian Institute of Technology (BHU),

Varanasi - 221005, (U.P.), India

Indian Institute of Technology (BHU)  
भारतीय प्रौद्योगिकी संस्थान (का०हि०वि०वि०)  
Varanasi-221005/वाराणसी-221005

**Anil Kumar**

Dr. Anil Kumar

Co-Supervisor

Associate Professor

Department of Ceramic Engineering,

Indian Institute of Technology (BHU),

Varanasi - 221005, (U.P.), India

Indian Institute of Technology (B.H.U.)

भारतीय प्रौद्योगिकी संस्थान (का०हि०वि०वि०)

Varanasi-221005/वाराणसी-221005

**Prof. Vinay Kumar Singh**

Head of Department

Department of Ceramic Engineering,

Indian Institute of Technology (BHU)

Varanasi - 221005, (U.P.), India

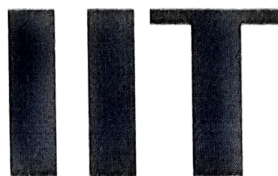
Indian Institute of Technology (B.H.U.)

भारतीय प्रौद्योगिकी संस्थान (का०हि०वि०वि०)

Varanasi-221005/वाराणसी-221005



भारतीय  
प्रौद्योगिकी  
संस्थान  
वाराणसी हिन्दू विश्वविद्यालय



INDIAN  
INSTITUTE OF  
TECHNOLOGY  
BANARAS HINDU UNIVERSITY

---

## COPYRIGHT TRANSFER CERTIFICATE

**Title of the Thesis:** *Tuning of Redox energies of transition metal ions in different lattices for grid-scale energy storage applications"*

**Name of the Student:** *Rakesh Mondal*

### Copyright Transfer

The undersigned hereby assigns to the Indian Institute of Technology (Banaras Hindu University) Varanasi all rights under copyright that may exist in and for the above thesis submitted for the award of the "*DOCTOR OF PHILOSOPHY*".

Date: 02/08/2022

Place: IIT (BHU), Varanasi

*Rakesh Mondal*  
Signature of the Student  
(*Rakesh Mondal*)

**Note:** However, the author may reproduce or authorize others to reproduce material extracted verbatim from the thesis or derivative of the thesis for the author's personal use provided that the source and the Institute's copyright notice are indicated.

## **Acknowledgement**

The journey toward Ph.D. has been a turning point in my life, and it would not be possible without the constant support, assistance, and guidance that I have received from countless people. I would like to take this opportunity to acknowledge and appreciate those people who have given their valuable time during my Ph.D. I am indebted to my thesis supervisor Dr. Preetam Singh for his constant monitoring, enthusiastic encouragement, continued guidance, and unconditional support throughout my Ph.D. journey. I always admire his knowledge of the subject, his unconventional thinking, and his enthusiastic nature for research. His ingenious approach to research is a source of inspiration, and this approach is reflected in his simple but clear writing style, which I want to carry forward in my career. I have been fortunate enough to be part of his group. His suggestions and advice will always be beneficial in life, whether it is academic or nonacademic. I am very thankful to you sir for being a mentor academically as well as philosophically and wish to continue to seek this mentorship in future life too.

I am thankful to my RPEC members, Prof. Rajiv Prakash (SMST, IIT-BHU), Dr. Anil Kumar, and Dr. Ram Pyare, for their knowledgeable, motivational, and umpteen suggestions throughout this research work. I want to express my gratitude to the Ex-Head of Department, Prof. D. Kumar, and Head of Department Prof. Vinay Kumar Singh for providing me required facilities of the department. I also wish to thank all the faculty members of the Department of Ceramic Engineering, Prof. D. Kumar, Prof. Om Prakash, Prof. S.P. Singh, Prof. Ram Pyare, Prof. Vinay Kumar Singh, Dr. Preetam Singh, Dr. Anil Kumar, Dr. M. R. Majhi, Dr. P. K. Roy, Dr. Ashutosh Dubey, Dr. Santanu Das, Dr. Imteyaz Ahmed, Dr. Sudama Singh, Dr. R.K. Chaturvedi, for their motivation, selfless support, a suggestions during course work as well as my whole Ph.D. time. I would also like to thank Prof. Rajiv Prakash for providing experimental facilities during the entire course of research work at CIFIC, IIT (BHU). Along with that, I am also thankful to all the staff at CIFIC, IIT(BHU).and Prof. Rajiv Prakash (SMST, IIT-BHU), Dr. T. Maiyalagan Department of Chemistry, SRM University Chennai, for their valuable discussions over the scientific work.

I would like to extend thanks to Dr. Asha Gupta, Department of Chemistry IIT(BHU) for providing a lab facility during the time of crisis. I also gratefully acknowledge the financial support of the Ministry of Education, India (formally known as the Ministry of Human Resource and Development; MHRD, India).

I am also thankful to all non-teaching staff, Mr. Shailendra, Mr. Pawan, Mr. Prasant, Mr. K. K. Maurya, (office staff)Mr. Ashish Tripathi, Mr. BhagmalJi, Mr. Mansa Ram(all Technical and workshop staff)of the Department of Ceramic Engineering for their kind cooperation. I am very thankful to the labmates Akanksha, Neeraj, Krishna Gopal Nigam, Neeraj, Himanshu, and for cooperating and maintaining the lab culture. I wish to express my sincere gratitude to all those who have extended their helping hands in various ways during my tenure at the Indian Institute of Technology (Banaras Hindu University), Varanasi, India. I am also thankful for the negative energies which teach me life lessons and help me to grow.

I am highly obliged to my parent and my family, for their continuing support, love, laughter, and motivation to keep me coherent and to make this project possible especially during many rough patches of time I would like to mention my friend Dibyajyoti Mohanta, Bishnu pada majhi, Chinmoy Rajak, Uttam Sarkar, Kallol Sarkar, etc. for having that emotional and motivational support during the tenure. Lastly, I want to thank almighty God for all positive opportunities and negative situations which prepare me to handle situations in the future life

## **Table of Contents**

List of Figures .....	xi
List of Tables .....	xxiii
List of Abbreviations .....	xxiv
Preface.....	xxv
<b>Chapter 1: Introduction</b>	
1.1 Global warming and energy security.....	1
1.1.1 Global warming and Climate change .....	1
1.1.1.1 Global warming.....	1
1.1.1.2 Climate change.....	2
1.1.1.3 Causes of climate change .....	3
1.1.2 Energy security .....	3
1.2 Pollution control and green energy over fossil .....	4
1.3 Renewable energy and alternative energy solutions .....	5
1.4 Limitation/ problem with Renewable energy .....	6
1.5 Type of energy storage solutions.....	6
1.5.1 The battery is an alternating grid-scale energy storage solution....	8
1.5.2 Limitation of conventional metal-ion (Li-ion and Na -ion) battery.....	9
1.6 Parameters of performances for grid-scale energy storage .....	9
1.6.1 Redox flow battery technology for grid-scale energy storage application...	10
1.6.2 Metal-sulphur battery technology for grid-scale energy storage application...	11
1.6.3 Metal-air battery technology for grid-scale energy storage application....	13
1.6.3.1 Development of metal-air battery .....	14
1.6.3.2 Type Metal-air batteries .....	15
1.6.3.3 Metal anode and Working principle of the metal-air battery .....	16
1.6.3.4 Air cathode and role of cathode supported OER (Oxygen Evolution Reaction) and (Oxygen Reduction Reaction) ORR catalyst .....	17
1.6.3.4 .1 Overpotential .....	18
1.6.3.4 .2 Tafel slope .....	19
1.6.3.4 .3 Exchange current density ( $i_0$ ) .....	19

1.6.3.5 Survey of OER (Oxygen Evolution Reaction) and (Oxygen Reduction Reaction)ORR catalysts with different lattice structures .....	20
1.6.3.5.1 OER and ORR activity of transition/noble metal oxides .....	21
1.6.3.5.2 Role of $e_g$ electron on ORR/OER activity of Spinel and perovskite-type Oxide materials .....	21
1.6.3.5.3 Role of $e_g$ electron on ORR activity of Perovskites ( $ABO_3$ ) metal oxides .....	24
1.7 Pseudocapacitors or Supercapacitors for grid-scale energy storage Application .....	25
1.7.1 Development of pseudocapacitors.....	26
1.7.2 Classification of Pseudocapacitance .....	27
1.7.3 Pseudocapacitive materials with different lattice structure.....	28
1.7.3.1 .1 Fe- $O_x$ redox mediator type materials .....	28
1.7.3.2 .2 VO $_x$ -based redox mediator type materials.....	29
1.7.3.3 .3 MnO $_x$ -based redox type materials .....	29
1.7.3.4 RuO $_2$ -based Redox mediator type materials .....	29
1.7.3.5 CoO $_x$ -based Redox mediator type materials.....	29
1.7.3.6 TiO $_2$ (B) cationic intercalation type materials .....	30
1.7.3.7 T-Nb $_2$ O $_5$ cationic intercalation type materials .....	30
1.7.3.8 Perovskite Oxides anionic intercalation type materials.....	31
1.8 Materials showing both OER/ORR catalysis and pseudocapacitance.....	32
References .....	35

## Chapter 2: Synthesis and Characterization Techniques

2.1 Overview .....	49
2.2 Materials Synthesis techniques.....	49
2.2.1 Solid-state or Ceramic method .....	50
2.2.2 sol-gel auto combustion method.....	50
2.2.3 Co-precipitation method.....	51
2.3 Characterization Techniques .....	52
2.3.1 X-ray Diffraction (XRD).....	52
2.3.2 High-Resolution Scanning Electron Microscope (HR-SEM).....	54
2.3.3 High-Resolution Transmission Electron Microscope (HR-TEM).....	56



2.3.4 Thermogravimetric analysis (TGA).....	58
2.3.5 Fourier transform infrared (FTIR) spectroscopy.....	58
2.3.6 UV-Visible Spectrophotometer.....	60
2.3.7 Raman Spectroscopy.....	61
2. 3.8 X-ray Photoelectron Spectroscopy (XPS).....	62
2.3.9 BET (Brunauer, Emmett, and Teller) specific surface area analysis.....	64
2.4 Electrode Fabrication and Cell Assembly.....	65
2.4.1 Electrode fabrication.....	65
2.4.2 Cell Assembly.....	66
2.4.3 Electrochemical characterization techniques.....	67
2.4.3.1 Linear sweep voltammetry (LSV).....	67
2.4.3.2 Cyclic voltammetry (CV).....	68
2.4.3.3 Chemical Kinetic of pseudocapacitors from cyclic voltammetry curve...	69
2.4.3.4 Charge-discharge (Chronopotentiometry).....	71
2.4.3.5 Electrochemical Impedance Spectroscopy (EIS).....	73
References.....	75

**Chapter-3: Ni stabilized Rock-Salt structured CoO; Co<sub>1-x</sub>Ni<sub>x</sub>O: Tuning of e<sub>g</sub> electrons to Development a Novel OER Catalysts**

3.1 Introduction.....	79
3.2 Materials Synthesis and characterizations.....	80
3.2 .1 Electrochemical Studies.....	81
3.3 Results and Discussion.....	82
3.3.1 XRD and Crystal structure.....	82
3.3.2 SEM analysis.....	83
3.3.3 Fourier transform infrared spectroscopy (FTIR) analysis.....	84
3.3.4 X-ray photoelectron spectroscopy (XPS) analysis.....	84
3.3.5 Linear Swept voltammetry (LSV) and Electrochemical Impedance Spectroscopy (EIS) analysis 1M KOH electrolyte.....	85

3.3.6 Linear Swept voltammetry (LSV) and EIS measurements in different molar KOH electrolyte .....	87
3.3.7 Linear Swept voltammetry and EIS measurements in 5M KOH electrolyte .....	87
3.3.8 Comparative Tafel slope in 1M and 5M KOH.....	88
3.3.9 Showing stability of OER catalyst in 5M KOH.....	91
3.3.10 Role of eg electrons on OER and ORR catalyst.....	91
3.4 Conclusions.....	93
References.....	94

## **Chapter 4: Investigation of Role of Sr and Development of Superior Sr doped Hexagonal**

### **BaCoO<sub>3-δ</sub> Perovskite Bifunctional OER/ORR Catalyst in Alkaline**

#### **Media**

4.1 Introduction .....	99
4.2 Materials Synthesis and characterization.....	100
4.2.1 Electrochemical Studies.....	101
4.3 Results and Discussion .....	102
4.3.1 Crystallographic characterization.....	102
4.3.2 Brunauer-Emmett-Teller (BET) analysis.....	104
4.3.3 Scanning Electron Microscopy (SEM) with Energy Dispersive X-Ray Analysis (EDX) analysis .....	104
4.3.4 Transmission electron microscopes (TEM) analysis .....	105
4.3.5 X-ray photoelectron spectroscopy (XPS) analysis.....	106
4.3.6 Temperature-dependent resistivity study.....	107
4.3.7 UV visible spectroscopy analysis.....	108
4.3.8 Electronic structure.....	108
4.3.9 Role of Sr doped in BaCoO <sub>3</sub> .....	110
4.3.10 Mott–Schottky and flat-band potential.....	110
4.3.11 Linear Sweep Voltammetry (LSV) analysis.....	111
4.3.12 EIS (Electrochemical impedance spectroscopy) analysis .....	113
4.3.13 Cyclic voltammetry perform in different concentration electrolytes.....	113

4.3.14 Stability perform cyclic voltammetry analysis .....	114
4.3.15 Stability test by chronoamperometric experiment.....	115
4.4 Conclusion.....	116
References.....	117

**Chapter 5:  $\text{La}_{0.5}\text{K}_{0.5}\text{CoO}_{3-\delta}$  ( $0 \leq x \leq 0.5$ ) Perovskite: A Novel Bifunctional OER catalyst and supercapacitive energy storage material**

5.1 Introduction .....	123
5.2 Materials Synthesis and characterizations .....	124
5.2.1 Electrode fabrication.....	125
5.2.2 Electrochemical Studies .....	126
5.2.2.1 Electrocatalysts measurement.....	126
5.2.2.2 Supercapacitors measurement.....	127
5.3 Results and discussions .....	127
5.3.1 Crystallographic characterization.....	127
5.3.2 FTIR spectra analysis.....	128
5.3.3 UV-vis absorption spectrum and bandgap analysis.....	130
5.3.4 BET surface area and pore size analysis.....	130
5.3.5 XPS analysis.....	131
5.3.6 SEM analysis.....	132
5.3.7 TEM analysis.....	133
5.3.8 Strain-induced distortion of $\text{CoO}_5$ octahedra.....	134
5.3.9 Double-exchange of $\text{Co}^{3+}-\text{O}^{2-}-\text{Co}^{4+}$ .....	134
5.3.10 Co (3d)/O (2p) orbital overlap.....	135
5.3.11 Mott–Schottky plot.....	136
5.3.12 Linear Sweep Voltammetry (LSV) analysis.....	137
5.3.13 EIS (Electrochemical impedance spectroscopy) and Cdl value analysis	139
5.3.14 Chronoamperometric stability test.....	139
5.4 Electrochemical Charge Storage Behaviour in neutral $\text{Na}_2\text{SO}_4$ electrolyte....	140
5.4.1 Bifunctional OER catalyst and supercapacitive energy storage behavior....	140
5.4.2 Cyclic voltammetry study in neutral $\text{Na}_2\text{SO}_4$ electrolyte... ..	141
5.4.3 b value (Kinetics) in $\text{Na}_2\text{SO}_4$ aqueous electrolyte .....	143
5.4.4 Dunn method and Kinetics analysis.....	143

5.4.5 Charge discharge (plot V vs. time) analysis in Na <sub>2</sub> SO <sub>4</sub> aqueous electrolyte.....	145
5.4.6 EIS analysis in Na <sub>2</sub> SO <sub>4</sub> Aqueous electrolyte.....	146
5.4.7 Full cell (La <sub>0.5</sub> K <sub>0.5</sub> CoO <sub>3-δ</sub> // AC (Activated carbon) electrochemical Analysis in Na <sub>2</sub> SO <sub>4</sub> aqueous electrolyte.....	147
5.4.8 Full cell (La <sub>0.5</sub> K <sub>0.5</sub> CoO <sub>3-δ</sub> // AC (Activated carbon) EIS (Electrochemical Impedance Spectroscopy) analysis in Na <sub>2</sub> SO <sub>4</sub> aqueous electrolyte .....	148
5.4.9 Full cell (La <sub>0.5</sub> K <sub>0.5</sub> CoO <sub>3-δ</sub> // AC (Activated carbon) of specific energy vs. Specific power in Na <sub>2</sub> SO <sub>4</sub> aqueous electrolyte .....	149
5.5 Conclusions.....	150
References.....	151

**Chapter 6: La<sub>1-x</sub>K<sub>x</sub>FeO<sub>3-δ</sub>: An anion intercalative pseudo-capacitive electrode for supercapacitors application**

6.1 Introduction.....	157
6.2 Materials Synthesis and characterizations.....	159
6.2.1 Electrochemical Studies .....	160
6.3 Results and Discussions .....	160
6.3.1 Crystallographic characterization.....	160
6.3.2 X-ray photoelectron spectroscopy (XPS) analysis .....	162
6.3.3 Brunauer-Emmett-Teller (BET) analysis.....	163
6.3.4 Scanning Electron Microscopy (SEM) with Analysis (EDX) and High-Resolution Transmission Electron Microscopes (HRTEM) analysis.....	164
6.3.5 Cyclic Voltammetry analysis.....	165
6.3.6 Determination of the Diffusion coefficient .....	167
6.3.7 Determination of b values and analysis .....	168
6.3.8 Dunn's plot analysis.....	170
6.3.9 Trassati's plot analysis.....	171
6.3.10 Chronoamperometry (charge-discharge).....	172
6.3.11 Electrochemical impedance spectroscopy (EIS) analysis.....	173
6.3.12 Two electrodes full cell test of La <sub>0.5</sub> K <sub>0.5</sub> FeO <sub>3-δ</sub> //AC (CV, charge-discharge, and cyclic stability).....	174
6.3.13 Electrochemical impedance spectroscopy of two electrodes	

(La <sub>0.5</sub> K <sub>0.5</sub> FeO <sub>3-δ</sub> //AC full cell) .....	176
6.3.14 Study of specific energy vs. specific power of full cell	
(La <sub>0.5</sub> K <sub>0.5</sub> FeO <sub>3-δ</sub> //AC full cell).....	177
6.4 Conclusions.....	178
References.....	179

**Chapter 7: Anhydrous NiC<sub>2</sub>O<sub>4</sub> Quantum dots: A superior pseudocapacitive electrode for large-scale energy storage applications in aqueous KOH and neutral Na<sub>2</sub>SO<sub>4</sub> electrolyte**

7.1 Introduction.....	185
7.2 Material Synthesis and Characterizations.....	186
7.2.1 Preparation of Electrode.....	188
7.3 Results and Discussions.....	188
7.3.1 Crystallographic characterization.....	188
7.3.2 Thermo-gravimetric Analysis (TGA) and Differential thermal Analysis (DTA).....	190
7.3.3 Fourier transform infrared spectroscopy (FTIR) analysis .....	191
7.3.4 Brunauer-Emmett-Teller (BET) surface area analysis.....	192
7.3.5 Raman spectrum analysis.....	193
7.3.6 UV visible spectroscopy analysis.....	194
7.3.7 X-ray photoelectron spectroscopy (XPS) analysis.....	194
7.3.8 High-resolution scanning electron microscopy (HRSEM) analysis .....	196
7.3.9 High-resolution scanning electron microscopy (HRSEM) analysis .....	196
7.3.10 Cyclic Voltammetry analysis.....	197
7.3.11 Determination of Diffusion coefficient .....	199
7.3.12 Determination of b values and analysis .....	200
7.2.13 Dunn's plot analysis.....	201
7.3.14 Trassati's plot analysis.....	203
7.3.15 Chronoamperometry Charge -discharge analysis.....	204
7.3.16 Electrochemical impedance spectroscopy (EIS) analysis.....	206
7.3.17 Full cell cyclic voltammetry (CV) of Activated carbon // of NiC <sub>2</sub> O <sub>4</sub> .2H <sub>2</sub> O QDs and NiC <sub>2</sub> O <sub>4</sub> QDs in 2M KOH analysis .....	207

7.3.18 Full cell charge-discharge of Activated carbon // NiC <sub>2</sub> O <sub>4</sub> .2H <sub>2</sub> O QDs and NiC <sub>2</sub> O <sub>4</sub> QDs in 2M KOH analysis and stability of AC// NiC <sub>2</sub> O <sub>4</sub> QDs after 2500 cycles.....	208
7.3.19 Comparative Electrochemical impedance spectroscopy (EIS) Analysis Activated carbon // of NiC <sub>2</sub> O <sub>4</sub> .2H <sub>2</sub> O QDs and NiC <sub>2</sub> O <sub>4</sub> QDs in 2M KOH analysis.....	209
7.3.20 NiC <sub>2</sub> O <sub>4</sub> QDs electrochemical analysis in 1M Na <sub>2</sub> SO <sub>4</sub> .....	210
7.3.21 Full cell AC// NiC <sub>2</sub> O <sub>4</sub> QDs electrochemical analysis in 1M Na <sub>2</sub> SO <sub>4</sub> .....	211
7.3.22 Comparative Power Density vs. Energy Density of AC// NiC <sub>2</sub> O <sub>4</sub> QDs in 2M KOH and 1M Na <sub>2</sub> SO <sub>4</sub> .....	212
7.4 Conclusions.....	213
References.....	215
<b>Chapter 8: Summary and Future scope</b>	
8.1 Summary .....	221
8.2 Future Scope .....	223

## List of Figure

---

Figure No.	Figure description	Page No.
Figure 1.1	Illustration of Global Warming	2
Figure 1.2	Causes of global warming and Climate change	2
Figure 1.3	Concept of energy security	4
Figure 1.4	a) Source of renewable energy b) Breakdown of renewables use in total final energy consumption terms	5
Figure 1.5	Different types of grid energy storage technologies for stationary applications	6
Figure 1.6	different types of energy storage technologies for stationary applications	7
Figure 1.7	. a) Schematic illustration of the first Li-ion battery (LiCoO <sub>2</sub> /Li <sup>+</sup> -ion electrolyte/graphite) b) Gravimetric power and energy densities for different rechargeable batteries	8
Figure 1.8	Suitability of energy storage technologies to different power and rate of discharge requirements	10
Figure 1.9	Schematic of the mechanism of vanadium redox flow battery	11
Figure 1.10	Schematic diagrams of Li-S cell with its charge/discharge operations	12
Figure 1.11	Schematic diagrams of Li-air battery	14
Figure 1.12	Theoretical energy density, specific energy, and nominal cell voltage of different types of metal-air batteries	15
Figure 1.13	Schematic diagrams of Metal-Air Batteries working principles for (a) non-aqueous electrolyte, and (b) aqueous electrolyte	16
Figure 1.14	Schematic diagrams of a) working principle of Zn-air battery and b) OER and ORR mechanism on air cathode	18
Figure 1.15	Schematic diagrams of Gibbs free energy of reactive species and intermediates (horizontal lines) of the oxygen evolution reaction (OER) versus the reaction coordinate. Blue lines and red lines indicate the energetics of a real (typical) catalyst and an ideal catalyst	20

Figure 1.16	Schematic diagrams of Volcano plots of common metal electrocatalysts	21
Figure 1.17	(a-b) Schematic diagrams of Volcano plots ORR and OER activity respectively on various spinel's as a function of $e_g$ occupancy of the active element at the octahedral site	22
Figure 1.18	Electronic configurations (d orbital spitting bonding ( $t_{2g}$ )) and antibonding ( $e_g$ )) and relevant metal orbitals of first-row transition metals for a $BO_5$ configuration	23
Figure 1.19	The relation between the OER catalytic activity, defined by the overpotentials at $50 \mu A cm^{-2}$ of OER current, and the occupancy of the $e_g$ -symmetry electron of the transition metal (B in $ABO_3$ )	23
Figure 1.20	a) Potentials at $25 mA/cm^2$ of the perovskite oxides have an M-shaped relationship with the d electron number b) Role of $e_g$ electron on ORR activity of perovskite oxides, Potentials at $25 mA/cm^2$ as a function of $e_g$ orbital in perovskite-based oxides	24
Figure 1.21	Advantage of supercapacitors over battery	25
Figure 1.22	Timeline of major developments in the field of pseudocapacitance	26
Figure 1.23	a) Adsorption pseudocapacitance, b) redox pseudocapacitance, and c) intercalation pseudocapacitance. d) CV of a Pt. (110) surface in aqueous $0.1M HClO_4$ solution at $50mV/s$ E) CV of a $RuO_2 \cdot 0.5H_2O$ electrode in aqueous $0.5M H_2SO_4$ solution f) CV of T- $Nb_2O_5$ Nano crystalline film in a nonaqueous $Li^+$ electrolyte cycled at $0.1 mV/s$ .	28
Figure 1.24	Structural model of T- $Nb_2O_5$ , highlighting densely packed 4h layers and loosely packed 4g layers and proposed low-hindrance $Li^+$ diffusion paths between bridging sites Nyquist Plot for ionic solids	30
Figure 1.25	shows $O^{2-}$ intercalation in $SrCoO_{3-\delta}$	31
Figure 1.26	a) LSV collected at $5 mV s^{-1}$ for NiO-NFBs, NiO-NPTs, and Ni foam electrodes, b) respective Tafel slopes c) CV of NiO nanoparticles film on nickel foams working electrode in $1M KOH$ d) Galvanostatic charge/discharge profiles for NiO nanoparticles film on nickel in the potential range of $0-0.5V$	33



Figure 1.27	a) morphology MnO <sub>2</sub> b) LSV -curves MnO <sub>2</sub> -based samples on Ni foam c ) CV curves at various scan rates (the inset is the CV curve at 5 mV s <sup>-1</sup> ), d) galvanostatic charge-discharge curves at various current densities of MnO <sub>2</sub>	34
Figure 2.1	Schematic representation of the three types of synthesis routes	49
Figure 2.2	block diagram of the solid-state synthesis process	50
Figure 2.3	block diagram sol-gel auto combustion synthesis process	50
Figure 2.4	block diagram Co-precipitation synthesis process	52
Figure 2.5	Schematic diagram of the incident and diffracted X-rays from the crystal	53
Figure 2.6	Rigaku, Miniflex II, Japan, IIT (BHU) Varanasi	54
Figure 2.7	Schematic diagram of the core component of SEM microscope	55
Figure 2.8	HR-SEM Instrument facility, ZEISS EVO 18 in CIFIC IIT (BHU) Varanasi	55
Figure 2.9	(a) Schematic diagram of core component of TEM microscope. Transmitted and diffracted electrons for (b) Bright field and (c) Dark field imaging in TEM	57
Figure 2.10	HRTEM Facilities with EDAX spectrometer, IIT (BHU) Varanasi	57
Figure 2.11	TGA measurement system CIFIC, IIT (BHU) Varanasi	58
Figure 2.12	Brief mechanism of FTIR for detection	59
Figure 2.13	FTIR spectrometer CIFIC, IIT (BHU) Varanasi	60
Figure 2.14	Schematic diagram of UV-Visible spectrometer	60
Figure 2.15	Schematic representation of the scattering process in Raman scattering	61
Figure 2.16	Schematic diagram of Raman spectrometer.	62
Figure 2.17	Schematic diagram XPS Basic Principle	63
Figure 2.18	XPS Spectrometer, CIFIC. IIT(BHU) Varanasi	63
Figure 2.19	BET surface area measurement system, CIFIC, IIT (BHU) Varanasi	65
Figure 2.20	Electrode picture for supercapacitors application	66
Figure 2.21	An electrochemical cell in a three-electrode system	67
Figure 2.22	Linear sweep voltammetry (LSV) polarization curve, voltage(V) vs.	68

	current	
Figure 2.23	Cyclic voltammetry (CV) polarization curve , voltage(V) vs. current	69
Figure 2.24	Power-law dependence of the peak current on sweep rate for capacitive materials (b= 1.0) and typical battery-type materials (b = 0.5).	70
Figure 2.25	Charge-discharge (Chronopotentiometry) plot voltage vs. time	72
Figure 2.26	Electrochemical impedance spectroscopy (EIS) mechanism and cole-cole plot	74
Figure 3.1	(a). X-ray diffraction patterns of $Ni_xCo_{1-x}O$ ( $0 \leq x \leq 0.4$ ) denoted (b). Rietveld refinement of XRD pattern of $Ni_{0.3}Co_{0.7}O$	82
Figure 3.2	(a) Scanning electron micrograph of $Ni_{0.3}Co_{0.7}O$ . (b) Scanning electron micrograph (enlarged view) of $Ni_{0.3}Co_{0.7}O$ (c) EDX analysis showing the stoichiometric distribution of Co, Ni, and O elements	83
Figure 3.3	FTIR spectrum of $Ni_{0.3}Co_{0.7}O$	84
Figure 3.4	XPS of $Ni_{0.3}Co_{0.7}O$ . (a) Full XPS survey of $Ni_{0.3}Co_{0.7}O$ (b) Core level $Ni2p$ spectrum (c) $Co2p$ spectrum (d) $O1s$ spectrum	85
Figure 3.5	(a) OER activity of $Co_{1-x}Ni_xO$ at 1 M KOH electrolyte. (b) ORR activity of $Co_{1-x}Ni_xO$ at 1 M KOH electrolyte. (c) OER and ORR performed of $Ni_{0.3}Co_{0.7}O$ with mechanism (d) EIS measurements of $Co_{1-x}Ni_xO$ at 1 M KOH electrolyte	86
Figure 3.6	(a) OER activity of $Co_{0.7}Ni_{0.3}O$ from 1M to 6 M KOH electrolyte (b) EIS measurements of $Co_{1-x}Ni_xO$ at 1 M KOH electrolyte	87
Figure 3.7	(a) OER activity of $Co_{1-x}Ni_xO$ at 5 M KOH electrolyte. (b) ORR activity of $Co_{1-x}Ni_xO$ at 5 M KOH electrolyte. (c) EIS measurements of $Co_{1-x}Ni_xO$ at 5 M KOH electrolyte.	88
Figure 3.8	(a) Tafel plot of $Co_{1-x}Ni_xO$ at 1 M KOH. (b) Tafel plot of $Co_{1-x}Ni_xO$ at 5 M KOH	89
Figure 3.9	Showing stability of OER activity of $Ni_{0.3}Co_{0.7}O$ up to 200 cycles.	90
Figure 3.10	a) Volcano graph depicting correlation of $e_g$ electrons with overpotential (at 10 mA/ cm <sup>2</sup> ) and the Tafel slope at 1 M KOH electrolyte b) d orbital presentation and $e_g$ electron calculation	92

Figure 4.1	(a) powder xrd pattern of $Ba_{1-x}Sr_xCoO_{3-\delta}$ ( $0 \leq x \leq 0.5$ ), (b) Rietveld refinement XRD profile of $Ba_{0.5}Sr_{0.5}CoO_{3-\delta}$ (c) Vesta image of $Ba_{0.5}Sr_{0.5}CoO_{3-\delta}$ and (d) Represent of bond angle of Co-O-Co (between O-2p and Co-3d orbital)	102
Figure 4.2	N <sub>2</sub> adsorption/desorption isotherms of $BaCoO_{3-\delta}$ and $Ba_{0.5}Sr_{0.5}CoO_{3-\delta}$	104
Figure 4.3	(a) SEM image showing particle distribution (b) EDX elemental analysis	105
Figure 4.4	TEM image along with HRTEM showing lattice fringes and high-resolution FFT, inverse FFT with d spacing	105
Figure 4.5	(a) Full survey spectra of $Ba_{0.5}Sr_{0.5}CoO_{3-\delta}$ (b) core level of Ba (3d) and Co (2p) spectrum (c) core level of Sr(3d) spectrum (d) core level of O(1s) spectrum.	106
Figure 4.6	(a) The temperature dependence of electrical resistivity of the 2H-type solid solution $Ba_{1-x}Sr_xCoO_{3-\delta}$ ( $0 \leq x \leq 0.5$ ) as a function of Sr content (b) plot of $\ln(R)$ against $T^{-1/4}$ of the resistivity data	107
Figure 4.7	UV-vis absorption spectrum of $Ba_{1-x}Sr_xCoO_{3-\delta}$ ( $0 \leq x \leq 0.5$ ) powder sample	108
Figure 4.8	Scheme showing the presence of oxygen vacancies $BO_5$ octahedral with high overlapping between O(2p) and Co(3d) band.	109
Figure 4.9	Oxygen vacancies and pinning Fermi level at the top of the Co(3d)/O(2p) $\pi^*$ band	110
Figure 4.10	Scheme showing the presence of oxygen vacancies $BO_5$ octahedral with high overlapping between O(2p) and Co(3d) band. (c) Oxygen vacancies and pinning Fermi level at the top of the Co(3d)/O(2p) $\pi^*$ band	111
Figure 4.11	(a) OER and ORR polarization profiles of $Ba_{0.5}Sr_{0.5}CoO_{3-\delta}$ , (b) OER polarization profiles for the $Ba_{1-x}Sr_xCoO_{3-\delta}$ ( $0 \leq x \leq 0.5$ ) samples obtained using a $3 \text{ mVs}^{-1}$ scan rate, (c) in ORR polarization profiles for the $Ba_{1-x}Sr_xCoO_{3-\delta}$ ( $0 \leq x \leq 0.5$ ) samples obtained using a $3 \text{ mVs}^{-1}$ scan rate in O <sub>2</sub> saturated 0.1M KOH solution, (d) respective Tafel plots	112
Figure 4.12	electrochemical impedance spectra for the $Ba_{1-x}Sr_xCoO_{3-\delta}$ ( $0 \leq x \leq 0.5$ ) at 1.7V vs RHE	113

Figure 4.13	OER polarization profiles for the $\text{Ba}_{0.5}\text{Sr}_{0.5}\text{CoO}_{3-\delta}$ at $3 \text{ mVs}^{-1}$ scan rate in 0.1, 1, 3, 5, and 6M KOH	114
Figure 4.14	Cycles stability up to 500 cycles of $\text{Ba}_{0.5}\text{Sr}_{0.5}\text{CoO}_{3-\delta}$ electrode at $3 \text{ mVs}^{-1}$ in 1M KOH	115
Figure 4.15	Chronoamperometric responses of $\text{Ba}_{0.5}\text{Sr}_{0.5}\text{CoO}_{3-\delta}$ electrode at constant potentials at 1.7 V vs RHE at an initial current density of $10 \text{ mA/cm}^2$	115
Figure 5. 1	(a) XRD pattern of $\text{La}_{1-x}\text{K}_x\text{CoO}_{3-\delta}$ ( $0 \leq x \leq 0.5$ ), (b) Rietveld refinement of $\text{La}_{0.5}\text{K}_{0.5}\text{CoO}_{3-\delta}$ , (c) vesta image of $\text{La}_{0.5}\text{K}_{0.5}\text{CoO}_{3-\delta}$	127
Figure 5.2	FTIR spectra of $\text{La}_{1-x}\text{K}_x\text{CoO}_{3-\delta}$ ( $x=0, 0.3, 0.5$ )	129
Figure 5.3	(a) UV-vis absorption spectrum of $\text{La}_{1-x}\text{K}_x\text{CoO}_{3-\delta}$ ( $x=0, 0.3, 0.5$ ) (b) Optical bandgap of $\text{La}_{1-x}\text{K}_x\text{CoO}_{3-\delta}$ ( $x=0, 0.3, 0.5$ ).	130
Figure 5.4	$\text{N}_2$ adsorption/desorption isotherms of $\text{La}_{1-x}\text{K}_x\text{CoO}_{3-\delta}$ ( $x=0, 0.3, 0.5$ )	131
Figure 5. 5	XPS of $\text{La}_{0.5}\text{K}_{0.5}\text{CoO}_{3-\delta}$ of powder sample (a) full survey, (b) Fe(2p) core level, (c) O(1s), (d) La (3d) and (e) K(2p)	132
Figure 5.6	(a) SEM image showing particle distribution of $\text{La}_{0.5}\text{K}_{0.5}\text{CoO}_{3-\delta}$ (c) EDX elemental analysis of $\text{La}_{0.5}\text{K}_{0.5}\text{CoO}_{3-\delta}$	133
Figure 5.7	(a) TEM image along with HRTEM showing lattice fringes and high-resolution FFT, inverse FFT with d spacing (012 planes) of $\text{LaCoO}_3$ . (b) TEM image along with HRTEM showing lattice fringes and high-resolution FFT, inverse FFT with d spacing (012 planes) of $\text{La}_{0.5}\text{K}_{0.5}\text{CoO}_{3-\delta}$	133
Figure 5.8	Scheme showing the presence of oxygen vacancies $\text{BO}_5$ octahedral	134
Figure 5.9	Atomic orbital diagram of double-exchange $\text{Co}^{3+} - \text{O}^{2+} - \text{Co}^{4+}$ interaction	135
Figure 5.10	Oxygen Vacancies pinning Fermi level at the top of the $\text{Co}(3d)/\text{O}(2p) \pi^*$ band	136
Figure. 5.11	Mott-Schottky plot of p-type (hole) semiconductor $\text{La}_{1-x}\text{K}_x\text{CoO}_{3-\delta}$ ( $0 \leq x \leq 0.5$ ) and Flat band (Efb) potential	137
Figure 5.12	(a) OER polarization profiles of BSCF, $\text{Ba}_{0.5}\text{Sr}_{0.5}\text{CoO}_{3-\delta}$ , and $\text{La}_{0.7}\text{K}_{0.3}\text{CoO}_{3-\delta}$ in 1M KOH solution (b) OER polarization profiles for the $\text{La}_{1-x}\text{K}_x\text{CoO}_{3-\delta}$ ( $0 \leq x \leq 0.5$ ) samples obtained using a $3 \text{ mVs}^{-1}$ scan rate in 1M KOH solution (c) respective Tafel plots for $\text{La}_{1-x}\text{K}_x\text{CoO}_{3-\delta}$ ( $0 \leq x \leq 0.5$ ) sample (d) ORR polarization profiles for the $\text{La}_{1-x}\text{K}_x\text{CoO}_{3-\delta}$ ( $0 \leq x \leq 0.5$ ) samples obtained using a $3 \text{ mVs}^{-1}$ scan	138

	rate in O <sub>2</sub> saturated 1M KOH solution.	
Figure 5.13.	(a) Electrochemical impedance (EIS) spectra for the the La <sub>1-x</sub> K <sub>x</sub> CoO <sub>3-δ</sub> (0 ≤ x ≤ 0.5) at 1.7V vs RHE (b) measure Cdl values of La <sub>1-x</sub> K <sub>x</sub> CoO <sub>3-δ</sub> ( x = 0.1,0.3 and 0.5)	139
Figure 5.14	Chronoamperometric responses of La <sub>0.7</sub> K <sub>0.3</sub> CoO <sub>3-δ</sub> electrode at constant potentials at 1.7 V vs. RHE at an initial current density of 10 mA/ cm <sup>2</sup> . (Insert stability retention by CV	140
Figure 5.15	Cyclic voltammetry of La <sub>0.7</sub> K <sub>0.7</sub> CoO <sub>3-δ</sub> material at scan rate 10 mV/s in 1M KOH electrolyte and at scan rate 10 mV/s in 0.5 M Na <sub>2</sub> SO <sub>4</sub> electrolyte	141
Figure 5.16	(a) Comparative Cyclic voltammetry of La <sub>1-x</sub> K <sub>x</sub> CoO <sub>3-δ</sub> (0 ≤ x ≤ 0.5) material at scan rate 10 mV/s in 0.5 M Na <sub>2</sub> SO <sub>4</sub> electrolyte (b-d) cyclic voltammetry of La <sub>1-x</sub> K <sub>x</sub> CoO <sub>3-δ</sub> (x =0, 0.3, 0.5) material in in 0.5 M Na <sub>2</sub> SO <sub>4</sub> electrolyte	142
Figure 5.17	Plot of linear relationship between log (peak current) and log (scan rate) at two different scan rate regions of of La <sub>1-x</sub> K <sub>x</sub> CoO <sub>3-δ</sub> (x =0, 0.3, 0.5)	143
Figure 5.18	(a) Plot of power's law of charged state at a potential and discharged state at a potential of La <sub>1-x</sub> K <sub>x</sub> CoO <sub>3-δ</sub> (x =0, 0.3, 0.5) (b) Contribution of diffusive and capacitive at different scan rates contribution of of La <sub>1-x</sub> K <sub>x</sub> CoO <sub>3-δ</sub> (x =0, 0.3, 0.5) at 2mV/s	144
Figure 5.19	(a) Charge discharge (plot V vs. time) of La <sub>1-x</sub> K <sub>x</sub> CoO <sub>3-δ</sub> (0 ≤ x ≤ 0.5) electrode at 1A/g in 0.5 M Na <sub>2</sub> SO <sub>4</sub> (b) charge discharge (plot potential (V) vs. time(t) ) of La <sub>0.5</sub> K <sub>0.5</sub> CoO <sub>3-δ</sub> electrode 0.5M Na <sub>2</sub> SO <sub>4</sub> (c) capacitive retention and columbic efficacy with cycle -number	145
Figure 5.20	Impedance spectroscopy (EIS) at 10mV applied voltage(V) from 1MHz to 0.01 Hz	146
Figure 5.21	showing full cell (ASCs) performances of activated carbon vs. La <sub>0.5</sub> K <sub>0.5</sub> CoO <sub>3-δ</sub> electrode; (a) CV of individual electrodes at 10 mV/s respect to Hg/HgO electrode in 0.5 M Na <sub>2</sub> SO <sub>4</sub> , (b) CV at different scan rate of ASCs in 0.5 M Na <sub>2</sub> SO <sub>4</sub> (c) charge-discharge in 0.5 M Na <sub>2</sub> SO <sub>4</sub> , (d) Capacitance retention and coulombic efficiency with 2500 cycle at 10 A/g constant current of the full cell	147
Figure 5.22	showing EIS at 10 mV applied voltage, full cell (ASCs) performances of activated carbon vs. La <sub>0.5</sub> K <sub>0.5</sub> CoO <sub>3-δ</sub> electrode	149
Figure 5.23	showing Ragone plot full cell (ASCs) performances of activated carbon vs. La <sub>0.5</sub> K <sub>0.5</sub> CoO <sub>3-δ</sub> electrode	150
Figure 6. 1	(a) XRD pattern of La <sub>1-x</sub> K <sub>x</sub> FeO <sub>3-δ</sub> (x = 0, 0.1, 0.2, 0.3, 0.4, 0.5), (b) Rietveld	161

	refinement of $\text{La}_{0.5}\text{K}_{0.5}\text{FeO}_{3-\delta}$ , (c) structure of $\text{La}_{0.5}\text{K}_{0.5}\text{FeO}_{3-\delta}$ and (d) Jahn–Teller distortion over Fe-O octahedra in orthorhombic $\text{La}_{0.5}\text{K}_{0.5}\text{FeO}_{3-\delta}$ structure.	
Figure 6. 2	XPS of $\text{La}_{0.5}\text{K}_{0.5}\text{FeO}_{3-\delta}$ of powder sample (a) full survey, (b) Fe(2p) core level, (c) O(1s), (d) La (3d) and (e) K(2p)	163
Figure 6.3	show N <sub>2</sub> adsorption-desorption isotherms with the pore size distribution	164
Figure 6. 4	(a) SEM image showing morphology characteristic of $\text{La}_{0.5}\text{K}_{0.5}\text{FeO}_{3-\delta}$ and particles distribution from SEM image, (b) HRTEM image comprising the plane with distorted fringes (inset: FFT and inverse FFT of the selected region) of (002) plane and line profile of (002) plane the selected line in the inverse FFT image of the superstructural peak region.	164
Figure 6.5.	(a) Cyclic voltammetry of $\text{La}_{1-x}\text{K}_x\text{FeO}_{3-\delta}$ (x = 0, 0.4 and 0.5) material at scan rate 10 mV/s in 2M KOH electrolyte, ( b-d) cyclic voltammetry of $\text{La}_{1-x}\text{K}_x\text{FeO}_{3-\delta}$ (x = 0.3, 0.4, 0.5) material in 2M KOH electrolyte	166
Figure 6.6	Plot peak current density vs square root of scan rate of $\text{La}_{1-x}\text{K}_x\text{FeO}_{3-\delta}$ (x = 0, 0.3, 0.5) sample	167
Figure 6.7	(a-b) shows the linear relationship of log (v) vs log (i), slope represents the b value according to the power-law (c ) b value at the different potential of $\text{La}_{0.5}\text{K}_{0.5}\text{FeO}_{3-\delta}$ in charging and discharging process at a different potential, (d) plot of log(peak current) vs log(scan rate)	169
Figure 6.8	(a-b) capacitive and diffusion control processes contribution can be distinguished by the slope(k <sub>1</sub> ) and intercept(k <sub>2</sub> ) (c) capacitive and diffusion control process of $\text{La}_{0.5}\text{K}_{0.5}\text{FeO}_{3-\delta}$ electrode at 10mV/s, (d) capacitive and diffusion control percentage with different scan rate at discharge peak potential (-0.96V)	171
Figure 6.9	(a-b) corresponds to Trasatti plot at scan rate of 100mV/s to 1mV/s	172
Figure 6.10	a) Charge–discharge plot (V vs. time) of the $\text{La}_{1-x}\text{K}_x\text{FeO}_{3-\delta}$ (x = 0, 0.3, 0.4, 0.5) electrode at 1 A/g; (b) charge–discharge plot (potential (V) vs. time (t)) of the $\text{La}_{0.5}\text{K}_{0.5}\text{FeO}_{3-\delta}$ electrode; (c) capacitance performance of the $\text{La}_{0.5}\text{K}_{0.5}\text{FeO}_{3-\delta}$ 2 M KOH electrolyte at different constant currents; (d) capacitive retention and Coulombic efficiencywith cycle number	173
Figure 6.11	Electrochemical impedance spectroscopy (EIS) at 10 mV applied	174

	voltage from 1 MHz to 0.1 Hz.	
Figure 6.12	Full-cell (ASC) performances of activated carbon vs. the $\text{La}_{0.5}\text{K}_{0.5}\text{FeO}_{3-\delta}$ electrode. (a) CV of individual electrodes at 10 mV/s with respect to the Hg/HgO electrode; (b) CV at different scan rates of ASCs; (c) charge–discharge plot; (d) capacitance retention and Coulombic efficiency with 2000 cycles at 5 A/g constant currents of the full cell; and	175
Figure 6.13	Electrochemical impedance spectroscopy (EIS) at 10 mV applied voltage from 1 MHz to 0.1 Hz.	176
Figure 6.14	Ragone plot of the ASCs ( $\text{La}_{0.5}\text{K}_{0.5}\text{FeO}_{3-\delta}$ //AC) in full cell	177
Figure 7. 1	Schematic representation of synthesis process of $\text{NiC}_2\text{O}_4 \cdot 2\text{H}_2\text{O}$ and anhydrous $\text{NiC}_2\text{O}_4$ quantum dots (QDs)	187
Figure. 7.2.	(a) xrd pattern of $\text{NiC}_2\text{O}_4 \cdot 2\text{H}_2\text{O}$ QDs (b) anhydrous $\text{NiC}_2\text{O}_4$ QDs	189
Figure 7.3	TGA and DTA of bulk $\text{NiC}_2\text{O}_4 \cdot 2\text{H}_2\text{O}$ and $\text{NiC}_2\text{O}_4 \cdot 2\text{H}_2\text{O}$ QDs sample	190
Figure 7.4	FT-IR spectrums of $\text{NiC}_2\text{O}_4 \cdot 2\text{H}_2\text{O}$ QDs and anhydrous $\text{NiC}_2\text{O}_4$ QDs powder samples	191
Figure. 7.5	BET surface area measurements plot of $\text{NiC}_2\text{O}_4 \cdot 2\text{H}_2\text{O}$ QDs and $\text{NiC}_2\text{O}_4$ QDs	192
Figure 7.6	Raman shift of $\text{NiC}_2\text{O}_4 \cdot 2\text{H}_2\text{O}$ QDs and $\text{NiC}_2\text{O}_4$ QDs	193
Figure 7.7	a) UV absorbance of bulk and $\text{NiC}_2\text{O}_4$ QDs sample (b) bandgap of bulk and $\text{NiC}_2\text{O}_4$ QDs	194
Figure 7.8	XPS plot of (a) full survey $\text{NiC}_2\text{O}_4$ QDs (b) Ni (2p) spectrum and (c) Co 2p spectrum (d) O (1s) spectrum	195
Figure 7.9	HRSEM image showing the morphology and particle size distribution of (a) $\text{NiC}_2\text{O}_4 \cdot 2\text{H}_2\text{O}$ QDs (b) anhydrous $\text{NiC}_2\text{O}_4$ QDs, (c) EDX of anhydrous $\text{NiC}_2\text{O}_4$ QDs (d-f) elemental distribution of Ni, C, O of $\text{NiC}_2\text{O}_4$ QD	196
Figure. 7.10	HRTEM image at localized regions showing QDs of (a) $\text{NiC}_2\text{O}_4 \cdot 2\text{H}_2\text{O}$ QDs particle size with distribution (with FFT and inverse FFT) (b) calculating d-spacing of (202) plane (c) $\text{NiC}_2\text{O}_4$ QDs particle size with distribution (with FFT and inverse FFT) and (d) d-spacing of (110) plane.	197
Figure. 7.11	(a) Cyclic voltammetry of $\text{NiC}_2\text{O}_4 \cdot 2\text{H}_2\text{O}$ QDs (b) cyclic voltammetry	199

	of anhydrous NiC <sub>2</sub> O <sub>4</sub> QDs (c) comparative cyclic voltammetry of NiC <sub>2</sub> O <sub>4</sub> .2H <sub>2</sub> O QDs and NiC <sub>2</sub> O <sub>4</sub> .2H <sub>2</sub> O QDs at 10mV/s	
Figure 7.12	The plot of log(peak current vs. square root of scan rate of NiC <sub>2</sub> O <sub>4</sub> .2H <sub>2</sub> O QDs and NiC <sub>2</sub> O <sub>4</sub> QDs	200
Figure 7.13	b value of Plot of the linear relationship between log (peak current) and log (scan rate) of NiC <sub>2</sub> O <sub>4</sub> .2H <sub>2</sub> O QDs and NiC <sub>2</sub> O <sub>4</sub> QDs	201
Figure 7.14	(a Contribution of diffusive and capacitive at different scan rates contribution of NiC <sub>2</sub> O <sub>4</sub> QDs (b) Analysis of kinetic contribution at 10 mVs <sup>-1</sup> of NiC <sub>2</sub> O <sub>4</sub> QDs	202
Figure 7. 15	(a-b)Corresponding to Trasatti's plot of NiC <sub>2</sub> O <sub>4</sub> QDs	204
Figure 7.16.	(a) The comparative charge-discharge curve at 1A/g of NiC <sub>2</sub> O <sub>4</sub> 2H <sub>2</sub> O QDs and NiC <sub>2</sub> O <sub>4</sub> QDs (b-c) charge-charge curve of NiC <sub>2</sub> O <sub>4</sub> 2H <sub>2</sub> O QDs and NiC <sub>2</sub> O <sub>4</sub> QDsrespectively (d) capacitance performance of NiC <sub>2</sub> O <sub>4</sub> QDs at different constant current rates (e) capacitance retention and coulombic efficiency of porous NiC <sub>2</sub> O <sub>4</sub> QDs	205
Figure 7.17	EIS plot of NiC <sub>2</sub> O <sub>4</sub> .2H <sub>2</sub> O and porous NiC <sub>2</sub> O <sub>4</sub> QDs at 10mV (AC)	206
Figure. 7.18	plot for activated carbon and non-hydrate NiC <sub>2</sub> O <sub>4</sub> QDs cell in ASC mode (a) Compare single electrode CV of Activated Carbonvs.NiC <sub>2</sub> O <sub>4</sub> 2H <sub>2</sub> O QDs and NiC <sub>2</sub> O <sub>4</sub> QDs at 10 mV/s, in 2M KOH (b) compare Full cell CV both NiC <sub>2</sub> O <sub>4</sub> .2H <sub>2</sub> O QDs and NiC <sub>2</sub> O <sub>4</sub> QDs at 10 mV/s scan rates in 2M KOH, (c-d) Full cell CV of NiC <sub>2</sub> O <sub>4</sub> .2H <sub>2</sub> O and NiC <sub>2</sub> O <sub>4</sub> QDs at different scan rate charge-discharge in 2M KOH respectively	208
Figure. 7.19	(a) compare Full cell charge-discharge of both NiC <sub>2</sub> O <sub>4</sub> 2H <sub>2</sub> O QDs and NiC <sub>2</sub> O <sub>4</sub> QDs at 1A/g in 2M KOH (b-c) Full cell charge-discharge of both NiC <sub>2</sub> O <sub>4</sub> .2H <sub>2</sub> O QDs NiC <sub>2</sub> O <sub>4</sub> QDs at a different constant current in 2M respectively (d) Capacitance retention and coulombic efficiency of NiC <sub>2</sub> O <sub>4</sub> QDs in 2M KOH	209
Figure 7.20	shows a comparative EIS plot (Nyquist) of NiC <sub>2</sub> O <sub>4</sub> .2H <sub>2</sub> O QDs and anhydrous NiC <sub>2</sub> O <sub>4</sub> QDs in the frequency range (1MHz to 0.1Hz) at 10mV/s shows, that anhydrous NiC <sub>2</sub> O <sub>4</sub> QDs has higher charge transformation and higher diffusion behavior in the low-frequency region	209



- Figure 7.21 a) compare Full cell charge-discharge of both  $\text{NiC}_2\text{O}_4 \cdot 2\text{H}_2\text{O}$  QDs and  $\text{NiC}_2\text{O}_4$  QDs at 1A/g (b) compare Full cell charge-discharge of  $\text{NiC}_2\text{O}_4$  QDs at different constant current (c) EIS both  $\text{NiC}_2\text{O}_4 \cdot 2\text{H}_2\text{O}$  QDs and  $\text{NiC}_2\text{O}_4$  QDs at 10 mV(AC) 211
- Figure. 7.22 (a) Full cell CV  $\text{NiC}_2\text{O}_4$  QDs // Activated Carbon in 1M  $\text{Na}_2\text{SO}_4$  (b) Full cell charge-discharge of  $\text{NiC}_2\text{O}_4$  QDs in 1M  $\text{Na}_2\text{SO}_4$  at different constant current (c) EIS both  $\text{NiC}_2\text{O}_4 \cdot 2\text{H}_2\text{O}$  QDs and  $\text{NiC}_2\text{O}_4$  QDs at 10 mV(AC) (d) Capacitance retention and coulombic efficiency of  $\text{NiC}_2\text{O}_4$  QDs 212
- Figure 7.23 Ragone plot (Energy density vs. power density) of  $\text{NiC}_2\text{O}_4$  QDs in 2M KOH and 1M  $\text{Na}_2\text{SO}_4$  213

## List of tables

---

Table No.		Page No.
Table 1.1	Type of renewable energy source and application	5
Table 3.1	Structural Parameters of $\text{Ni}_x\text{Co}_{1-x}\text{O}$ ( $0 \leq x \leq 0.4$ )	83
Table 3.2	Tafel slope and Overpotential values of $\text{Ni}_x\text{Co}_{1-x}\text{O}$ ( $0 \leq x \leq 0.4$ ) at 1M and 5M KOH	90
Table 4.1:	lattice parameter of $\text{Ba}_{1-x}\text{Sr}_x\text{CoO}_{3-\delta}$ ( $0 \leq x \leq 0.5$ )	103
Table 5.1	lattice parameter of $\text{La}_{1-x}\text{K}_x\text{CoO}_{3-\delta}$ ( $0 \leq x \leq 0.5$ )	128
Table 6.1	Structural parameter of $\text{La}_{1-x}\text{K}_x\text{FeO}_3$ ( $0 \leq x \leq 0.5$ ) obtained Rietveld refinement	162
Table 6.2	Determination of diffusion coefficient	168

# LIST OF ABBREVIATIONS

---

XRD-X-ray Diffraction

HR-SEM-High Resolution Scanning Electron Microscopy

HR-TEM-High Resolution Transmission Electron Microscopy

TGA- Thermogravimetric analysis

FTIR-Fourier Transforms Infrared Spectroscopy

XPS-X-ray Photoelectron Spectroscopy

BET - (Brunauer, Emmett, and Teller) specific surface

LSV- Linear Sweep Voltammetry

CV- Cyclic Voltammetry

EIS- Electrochemical Impedance Spectroscopy

EDLC- Electric double layer capacitor

ASCs – Asymmetric Supercapacitors

AC-activated carbon

C<sub>sp</sub> - specific capacitance

E<sub>RHE</sub> – Potential respect to the Reversible Hydrogen Electrode

E<sub>fb</sub> - Flat Band Potential

OER -Oxygen Evolution Reaction

ORR -Oxygen Reduction Reaction

$\eta$  = overpotential

A = Tafel slope

$j$  = current density, mA/cm<sup>2</sup>

$j_0$  =Exchange current density", mA/cm<sup>2</sup>.

QDs- Quantum Dots

g-gram

A,mA- Ampere, milli-Ampere

# PREFACE

---

Energy storage is the biggest challenge the world is facing today in the 21<sup>st</sup> century to utilize the full potential of renewable energy sources such as solar, wind, Tidal, etc. to overcome the ever-increasing burden on fossil fuels to fulfill our power demands and to decrease the toxic release and net carbon addition to the environment resulting global warming due to burning of fossil fuels. Electrochemical Energy storage devices are also important to overcome power and current fluctuations associated with renewable energy sources to be utilized as power supply units in electric grids. Thus major attention in the energy storage device section is to develop a grid scale bulk energy storage and delivery system with superior energy storage and power delivering capabilities. Therefore redox flow batteries, Metal-air batteries, and hybrid supercapacitors are technologically important and materials development to enhance their capabilities is the major area of focus in the energy materials section.

- Bifunctional OER/ORR catalyst and pseudocapacitive electrode materials are important to develop bulk grid-scale energy storage and power delivering energy storage systems.
- Materials such as  $\text{RuO}_2$ ,  $\text{MnO}_2$ , and  $\text{NiOOH}$  become very important because they show superior electrocatalytic OER/ORR properties in basic media (KOH electrolyte) and Faradic pseudocapacitive storage in neutral or low pH aqueous electrolyte (KOH, KCl, and  $\text{Na}_2\text{SO}_4$  media).
- Perovskite such as  $\text{Ba}_{0.5}\text{Sr}_{0.5}\text{Co}_{0.8}\text{Fe}_{0.2}\text{O}_{3-\delta}$  (BSCF),  $\text{La}_{0.8}\text{Sr}_{0.2}\text{Co}_{0.8}\text{Fe}_{0.2}\text{O}_{3-\delta}$  (LSCF), and  $\text{LaNiO}_{3\pm\delta}$  are also known to have superior and stable electrocatalytic OER/ORR activity in aqueous high pH KOH electrolyte and recently pseudocapacitive anion charge-storage through oxygen intercalation was discovered in  $\text{LaMnO}_3$  perovskite electrodes.
- Thus there is a need to develop strategic understanding and guidelines to develop superior materials that can be employed as an electrode in both (1) metal-air batteries (as OER/ORR electrocatalyst) and (2) hybrid supercapacitors (pseudocapacitive charge storage electrode).
- Tuning redox properties with suitable crystal structure or lattice modification with novel doping or substitution strategies is important to achieve the

- Targeted electric and electronic properties in the material for the desired application. In this thesis, I attempted to map the electronic structure of the material with suitable doping of guest cations in the host lattice and draw a structure-property correlation in the materials to be applied for electrochemical energy storage application.

I have shown that the rock-salt structure can act as a model host structure similar to perovskite where  $e_g$  electrons can be varied to obtain superior electro-catalytic activity. Incorporation of Nickel into CoO lattices helps to stabilize the rock salt structure and tune the  $e_g$  electrons to develop superior OER and ORR electrocatalysts.  $Ni_{0.3}Co_{0.7}O$  with 1.3  $e_g$  electrons showed superior electrocatalytic activity for oxygen evolution reaction. Further, along with  $e_g$  electrons, I explored the role of Sr in  $Ba_{1-x}Sr_xCoO_{3-\delta}$  perovskite toward higher electrocatalytic OER/ORR activities and showed that the incorporation of Sr ion in  $Ba_{1-x}Sr_xCoO_{3-\delta}$  ( $0 \leq x \leq 0.5$ ) perovskite lattice, facilitates the formation of ligand hole by decreasing the Fermi level position into the  $Co(3d)/O(2p)\pi^*$  band. The decrease in the bandgap of the materials and superior electrical conductivity (p-type conduction) suggest a large number of oxygen vacancies or oxygen vacant  $BO_5$  octahedra formation that yields more active sites as this type of oxygen vacancy in perovskite lattice get more reaction surface or active sites because (011) plane contains transition metal (Co) in  $Ba_{1-x}Sr_xCoO_{3-\delta}$  perovskite that forms  $Co3d_{z^2}$  and  $OH-(2p_z+1s)$  bond.

Similar to multifunction  $RuO_2$  or  $MnO_2$  type materials, I have shown that  $La_{1-x}K_xCoO_{3-\delta}$  ( $0 \leq x \leq 0.5$ ) shows a pH-dependent bifunctional electrocatalyst (OER/ORR) and electrochemical charge storage behavior in different electrolytes. 30 % K doped p-type  $La_{0.7}K_{0.3}CoO_{3-\delta}$  show superior OER activity with an overpotential of 335 at  $10mA/cm^2$  current rate in 1M KOH electrolyte. Further, the double exchange mechanism enhances OER catalytic properties and additionally, improves charge storage kinetics and activities as electrode material  $La_{1-x}K_xCoO_{3-\delta}$  ( $0 \leq x \leq 0.5$ ) for supercapacitors application. High Gravimetric capacitance of  $La_{0.5}K_{0.5}CoO_{3-\delta}$  electrode equivalent to 378 F/g, 282F/g, 221F/g, 163F/g, 74F/g was found at a constant current of 1A/g, 2A/g, 3A/g, 5A/g, and 10A/g respectively in neutral 0.5M  $Na_2SO_4$  electrolyte with up to 94% capacitive retention and coulombic efficiency (97%).

An anion intercalative pseudo-capacitive  $La_{1-x}K_xFeO_{3-\delta}$  electrode for supercapacitors

application was developed using induced inter-layer potential by altering  $\text{La}^{3+}$  and  $\text{K}^+$  layer in  $\text{La}_{1-x}\text{K}_x\text{FeO}_{3-\delta}$ ,  $\text{Fe}^{4+/3+}$ , and  $\text{Fe}^{3+/2+}$  redox energies can be tuned and made accessible to envisage higher capacity (662 F/g equivalents to  $1.32 \text{ e}^-/\text{OH}^-$  diffusion) for  $\text{La}_{0.5}\text{K}_{0.5}\text{FeO}_{2.92}$  electrode. Higher b values ( $>0.8$ ) obtained for diffusion-controlled reaction suggest a high faradaic pseudocapacitive contribution to the electrode. Up to 88.6% capacitive retention and coulombic efficiency (95%) were obtained after continuous 5000 cycles of charge/discharge and Maximum specific power of  $\sim 3594 \text{ W/kg}$  was obtained when specific energy reached  $\sim 117 \text{ Wh/kg}$  at  $5 \text{ A/g}$  of current density for  $\text{La}_{0.5}\text{K}_{0.5}\text{FeO}_{3-\delta}$  electrode in two-electrode  $\text{La}_{0.5}\text{K}_{0.5}\text{FeO}_{3-\delta}/\text{AC}$  full cell.

Further Nano-engineering was employed to develop a superior pseudocapacitive electrode based on  $\text{Ni}^{2+/3+}$  redox couple in framework structure as Anhydrous  $\text{NiC}_2\text{O}_4$  Quantum dots that showed large-scale pseudocapacitive energy storage in aqueous KOH and neutral  $\text{Na}_2\text{SO}_4$  electrolyte. Predominant diffusion control over surface control mechanism seems to operate behind high charge storage as intercalative (Inner) and surface (outer) charges stored by porous anhydrous  $\text{NiC}_2\text{O}_4$  QDs were close to high at 38% and 62% respectively. Anhydrous  $\text{NiC}_2\text{O}_4$  QDs //AC full cell resulted in  $293 \text{ Wh/kg}$  of maximum specific energy with specific power equivalent to  $772 \text{ W/kg}$  in the voltage window of  $1.6 \text{ V}$  in  $2 \text{ M KOH}$  electrolyte.

Therefore in this thesis, I conclude the role of redox and tuning of redox energy with suitable cation doping in host perovskite lattice be employed as an efficient tool to alter its electrical and electronic properties so that the materials can show pH-dependent electrocatalytic (OER/ORR) properties and pseudocapacitive energy storage capabilities. The correlation of lattice structure and electronic state of active transition metal cation in the host lattice is established to develop novel OER/ORR catalyst and pseudocapacitive energy storage materials. This tuning of redox energies coupled with structure alteration can open the gate to explore novel new alternative materials for desired electrochemical energy storage applications